A Preliminary Study of Roughness Effects on a Compressible Turbulent Boundary Layer

Jonathan J. Gaskins*, Jonathan Poggie†, and Gregory Blaisdell‡
Purdue University, West Lafayette, Indiana, 47907-2045, USA

A preliminary computational study has been conducted regarding the effects of surface roughness on a compressible turbulent boundary layer. The study aimed to have large enough k^+ values to be in the fully rough regime, but low enough k/δ values to be considered flow over roughness and not flow over obstacles. The value of Re_{θ_i} was approximately $15,000$, and δ^+ was about 3800. From the flow visualization results, the roughness element tips appear to act as sources of low speed fluid in the process of mixing high and low-speed fluid. The roughness elements shelter the valleys of the elements, and alter the production of turbulence with adverse pressure gradients. The Reynolds stress values and mean velocity profiles do not match the results typically observed for rough-walls, that is a downward shifted magnitude of mean velocity and inner-scaled Reynolds stresses. The rough-wall case also has secondary peaks in the Reynolds stress plots which coincide with the area above the peaks of the roughness elements. These secondary peaks may suggest that the value of k/δ is not small enough, since the roughness elements are interfering with the buffer and logarithmic region. Further investigation into the choice of reference coefficient of friction is needed to determine if appropriate scaling of the calculated data was used.

I. Nomenclature

C	=	Y log-law constant
Cf	=	coefficient of friction
Cp	=	coefficient of pressure
k_s^+	=	roughness Reynolds number
u_τ	=	friction velocity
u_{vd}^+	=	van Driest and inner coordinates scaled mean velocity
y^+	=	wall-normal distance scaled by viscous length scale
δ	=	boundary layer thickness
δ_0	=	initial boundary layer thickness
δ^+	=	friction Reynolds number
κ	=	log-law inverse slope
ν/u_τ	=	viscous length scale
Ξ	=	diagnostic function

II. Introduction

In the pursuit of reusable high-speed vehicles, an improvement in the understanding of roughness effects on compressible turbulent boundary layers is necessary. High-speed vehicles are subject to the effects of roughness. The effects can include increased skin-friction, increased convective heat transfer, and transition to turbulence [1]. These effects have been studied extensively for incompressible boundary layers. Recent years have seen an increased number of studies for compressible boundary layers. Prior to discussing current literature regarding the rough-wall boundary layers studies, a few fundamental concepts will be presented in the following sections.

*Graduate Research Assitant, School of Aeronautics and Astronautics, gaskinsj@purdue.edu
†Professor, School of Aeronautics and Astronautics, jpoggie@purdue.edu, AIAA Associate Fellow
‡Professor, School of Aeronautics and Astronautics, blaisdel@purdue.edu, AIAA Associate Fellow

A. Turbulent Boundary Layer Structure

Wall-bounded turbulent flows consist of turbulent structures whose length scale can vary by orders of magnitude. The length scales of the structures typically increase as distance from the wall is increased. To coincide with the breadth of scales seen in turbulent flows, there are typically two regimes of scaling parameters. Variables described in inner coordinates are scaled by the friction velocity $u_\tau = (\tau/\rho)^{1/2}$ and the viscous length scale ν/u_τ. Values which are scaled using these parameters are denoted with a "+" superscript. In the region near the edge of the boundary layer, the main scaling parameter is δ , the thickness of the boundary layer. Variables scaled by δ are denoted by a bar. Inner coordinates are typically used for values of $\bar{y}$ less than 0.1 where y is the wall-normal direction.

Below $y^+ = 5$, viscous stress is typically dominant [2]. Between $y^+ = 10$ and $y^+ = 100$, a nonlinear self-sustaining cycle generates a large portion of turbulent energy [3]. This region is referred to as the buffer layer and it is characteristic of a transition from large viscous stresses to large Reynolds stresses [4]. If the outer and inner lengths have a large enough scale separation (characterized by a large enough value of δ^+), then there is a region where the relevant scaling parameter is the wall distance. This area is referred to as the logarithmic region due to the logarithmic distribution of the mean streamwise velocity [5]. The layer above the logarithmic region is referred to as the wake region. The wake region contains the outer layer dynamics with δ-scale structures.

B. Roughness

Jiménez [2] describes a few parameters which are important when defining roughness elements on a surface. The roughness Reynolds number k_s^+ is the equivalent sand grain roughness height scaled by the viscous length scale. A measure of the roughness elements direct effect on the buffer layer is k_s^+. Jimenez also defines two types of roughness elements, one of which is used in this study. D-type roughness elements are typically sized and spaced so that recirculation occurs between the elements. The roughness height and equivalent sand roughness height can largely vary for d-type roughness. K-type surfaces are typically sparser than d-rough surfaces and the dimensional size of k is proportional to the equivalent sand height. K-rough surfaces do not feature recirculation between elements. For this study, a k-rough surface is used. For this reason, k_s^+ will be called k^+.

A second parameter which is important to describing the sizing of roughness is k/δ. If k/δ is too large, the logarithmic layer can be destroyed, and the flow could be described more accurately as "flow over obstacles"[2]. Flows with too large a ratio do not retain the mechanisms of normal wall turbulence and can be very dependent on the roughness geometry.

According to Jiménez's review [2], there are unanswered questions in regard to rough-wall turbulent flows. A classical result of rough-wall studies is that the buffer layer can be perturbed without transmitting information to the outer flow besides a change of skin friction. One question which remains is if there are changes in length scales of turbulent structures between flat-wall and rough-wall cases. If there are significant changes in length scales, it could show that information is traveling from small scales to large scales. If there is information traveling from small to large scales, this could have implications for large-eddy simulations which assume there is little information flowing from small to large scales. A commonly seen shift in the oscillating streamwise velocity also suggests there are interactions not classically expected. To properly represent a rough surface which can answer these questions, k^+ should be in the fully rough regime where $k^+ > 50$. Values less than this are in the transitionally rough regime, where roughness effects are much more dependent on topology and shape. However, k should be small enough compared to the boundary layer to avoid blocking a significant portion of the logarithmic layer which leads to loss of the normal mechanisms of wall turbulence. A guideline set by Jiménez is that k/δ should be about 0.025. For both k^+ and k/δ values to be sufficient, δ^+ (the product of δ/k and k^+) should be at least 4000. This provides challenges for computational work, as the higher Reynolds number (δ^+) requirements leads to increased computation costs.

C. Recent Studies

Kocher et al. [6] provides a summary of important findings for incompressible and compressible rough-wall boundary layers. A few important findings which are relevant to the current study are discussed here.

Wu and Christensen [7][8][9] conducted studies related to the roughness induced on turbine blades in incompressible flow. They used high resolution PIV measurements to study an incompressible boundary layer over roughness elements. Their results showed a downward shift in the inner-scaled mean velocity profiles compared to a smooth wall. Reynolds stress values were shown to increase from the baseline case, particularly in regions of large roughness elements. The Reynolds stress profiles were found to collapse to the same profiles when scaled by friction velocity.

For compressible boundary layers, there have been several studies into roughness effects. Bowersox and Latin[10][11]

found that roughness elements in the fully rough regime reached into the supersonic region of the boundary layer, causing shock waves and expansion fans. Further studies aimed to simulate these roughness elements which caused shock waves and expansion fans [12][6][13]. Peltier and Bowersox [13] found that the roughness elements caused increased turbulent fluctuations in the lower half of the boundary layer, and decreased fluctuations in the upper half. Peltier and Bowersox [13] also found that the Reynolds stresses when scaled by friction velocity are lower in magnitude than the flat-wall case, which contradicts the collapsing proposed by Wu and Christensen [7][8][9] for incompressible flow.

These studies mostly aimed to replicate roughness elements seen in high-speed aircraft. The thermal protection systems of the high-speed aircraft shed material and produce an induced roughness which reaches into the supersonic region of flow. These studies are more specific to the roughness seen in these thermal protection systems and do not meet the guidelines set by Jiménez [2] for values of k^+ and k/δ to investigate flow physics between rough and flat-walls which obey similarity laws. In these studies there is a comparably large value of k/δ, which allows the roughness elements to perturb the supersonic region of the boundary layer. Jiménez describes flows with too large a ratio of k/δ as flows over obstacles. While they are practically useful for investigations into particular flow situations such as ablated thermal protection system roughness, there is a need for further insight into aspects of roughened-surface compressible boundary layers which obey similarity laws.

D. Objective of the Current Study

The goal of the current study is to investigate roughness effects of k-type roughness at a high enough Reynolds number (δ^+). The aim is to meet guidelines set by Jiménez to investigate aspects of compressible flows over surface roughness. The investigation uses a high-fidelity simulation utilizing the high-order solver Wabash (a new version of a code formerly known as HOPS [14]). Two baseline cases were ran, a flat-wall case and a rough-wall case.

III. Procedure

A. Numerical Methods

The Navier-Stokes equations for an ideal compressible gas are used to represent the physics of the flow. Transforming the variables in the conservation equations from physical coordinates x_i to grid coordinates ξ_i results in the following form of the equations:

$$\frac{\partial \bar{U}}{\partial t} + \frac{\partial \bar{E}_j}{\partial \xi_j} = \frac{\partial \bar{E}_j^{\nu}}{\partial \xi_j} + \bar{S} \tag{1}$$

In this form U is a solution vector represented as:

$$U = [\rho, \rho u_1, \rho u_2, \rho u_3, \varepsilon]^T \tag{2}$$

E_j is the inviscid flux vector. The viscous flux vector is E_j^{ν}. $\bar{U}$, $\bar{E}_j$, and $\bar{E}_j^{\nu}$ are transformed solution and flux vectors defined as:

$$\bar{U} = \frac{U}{J} \tag{3}$$

$$\bar{E}_i^{\nu} = \frac{\partial \xi_i}{\partial x_j} \frac{E_j}{J} \tag{4}$$

where J is the grid transformation Jacobian. These equations are solved using a spatial compact differencing scheme which is sixth-order at interior points and fourth-order at boundaries. For temporal discretization, an implicit method similar to the Beam-Warming Scheme [15] is used which provides second-order time accuracy. Higher-order methods are susceptible to numerical instabilities which can grow in the solution. To mitigate these instabilities, a low-pass non-dispersive filter is used after each time step.

B. Freestream Conditions and Wall Conditions

The freestream and wall conditions for the simulation can be seen in table 1. These conditions were selected to match those of the Mach 2 wind tunnel at the University of Tennessee Space Institute.

To maintain near adiabatic conditions at the wall, the wall temperature was kept constant at the adiabatic temperature of 266.0 K for the specified flow conditions. The simulation was initiated with a laminar similarity solution with the

Table 1 Freestream Conditions

P_∞(kPa)	T_∞(K)	U_∞ (m/s)	M_∞	δ_0 (m)	T_w (K)
26.4	158	506.0	2.01	5.0e-3	266.0

specified initial boundary layer thickness. The no-slip condition was imposed on the flat and rough surfaces of the generated grids. An artificial body-force trip was introduced at $x/\delta_0 = 2.5$ to promote transition to turbulence.

A nondimensional timestep ($U_\infty \Delta t/\delta_0$) of 5e-3 was used for the simulation. As discussed Poggie et al.[14], about 60,000 time steps were needed to reach a statistically steady state of the flow for this nondimensional time step.

C. Grid Generation

The grid dimensions were scaled accordingly with the initial boundary layer thickness ($\delta_0 = 5.0e-3$). The $x-$,$y-$, and $z-$ directions are defined as streamwise, surface-normal, and spanwise directions respectively. Two grids were generated, one with a smooth surface, and the other with a rough surface. The dimensions of both grids are seen in table 2 .

Table 2 Grid Dimensions

L_x/δ_0	L_y/δ_0	L_z/δ_0
100.0	6.0	6.0

Both grids were generated using an identical number of grid points in each direction. The streamwise direction was given a sponge layer of 25 grid points beyond $x = 100.0$. The wall normal was also given a sponge layer of 25 grid points beyond $y = 6.0$. The spanwise direction was given 6 overlap grid points starting at $z = 6.0$. The grid was generated so that the spacing in the wall normal direction grew with a constant stretching factor. The stretch factor was found by using a root finding function which would find the correct factor to fit the number of grid points desired in the wall-normal direction to the appropriate length of $y = 6.0$ with the specified initial wall spacing Δy_0. The flat-wall and rough-wall stretching factors were 1.023 and 1.027 respectively. Spacing of the grid points in the streamwise and spanwise direction was specified with a uniform spacing in the entire domain. The grid generation values without including sponge and overlap layers for the flat and rough-wall are specified in table 3 .

Table 3 Parameters describing the computational mesh.

i	j	k	Δy_0 rough	Δy_0 flat
8001	251	621	2.0e-4	4.5e-4

For the current study, resolving roughness elements appropriately is seen to be a limiting factor in roughness sizing, spacing, topology etc. As a baseline case, the roughness is defined as a sinusoidal plane, with an amplitude of k (the roughness height). The equation defining the roughness elements is as follows:

$$y = k \sin\left(2.0\pi \frac{x - x_0}{x_r}\right) \sin\left(2.0\pi \frac{z - z_0}{z_r}\right) \tag{5}$$

where $x_0 = 5.0$ (where the roughness elements start),$z_0 = 3.0$, $x_r = 2.5$, and $z_r = 0.5$. This equation yields a roughness pattern that resembles an egg carton. At $x = 100$, the roughness pattern ends and the wall becomes smooth. An image of the beginning of the rough grid with the start of the roughness elements can be seen in Fig. 1.

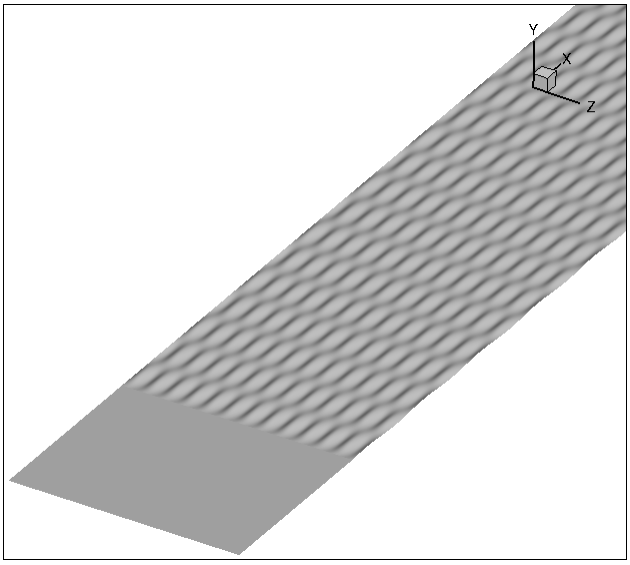

Fig. 1 Rough-wall surface.

D. Simulation Control and Data Logging

To induce turbulence into the solution of the domain of interest, an artificial body force trip located at the wall and centered at $x/\delta_0 = 2.5$ was used. The flow past this point transitions quickly to turbulence and a fully developed turbulent boundary layer.

To allow the flow to reach a statistically steady state, the simulation was run initially for 60,000 iterations. After 60,000 iterations, data were logged in 3 different planes. Data were logged for: the z-y plane at $x/\delta = 100$, the x-z plane for the length of x and from $z/\delta = 0$ to $z/\delta = 5.0$, and the x-y plane at approximately $z/\delta = 2.9$.

IV. Results

Table 4 shows the spatial resolution of each grid. Values specified are normalized with the viscous length scale. The values of $\delta^+$are close to the value recommended by Jiménez ($\delta^+ > 4000$) [2]. However, they do not exceed the targeted value. This will be discussed in a later section when the Reynolds stresses are shown. The value of $k^+ = 88.5$. The roughness at this value is considered to be in the fully-rough regime. The value of k/δ is 0.023. This marginally meets the value recommended by Jiménez (< 0.025)[2]. Jiménez suggested that the desired experimental value of k/δ may be closer to 0.0125. The value of k/x_r (ratio between the height of a roughness element and its length) is 0.04. The value of δ in table 4 is the boundary layer thickness at the end of the domain of interest ($x = 100$). The recommended values for LES according to Georgiadis et al. [16] is $50 \leq \Delta x^+ \leq 150$, $\Delta y_0^+ < 1$, and $15 \leq \Delta z^+ \leq 40$.

Table 4 Spatial Resolution and Reynolds Numbers

Case	Re_{θ_i}	δ^+	Δx^+	Δy_w^+	Δy_e^+	Δz^+	δ
Rough	15,400	3820	22	0.353	107	17.1	2.16
Flat	14,600	3750	22	0.796	90	17.1	2.12

A. Overall Flow Structure

To begin analyses of results, the flow was visualized through normalized density contours at the midpoint of the spanwise direction. Snapshots of these images can be seen in Fig. 2. In Fig. 2, δ represents the average thickness of the boundary layer at the end of the computational domain for the rough-wall case. Inflow of high-density freestream fluid into the near wall region can be seen in both cases. There are also expulsions of lower density fluid into the free-stream region up to about $\delta = 1.3$.

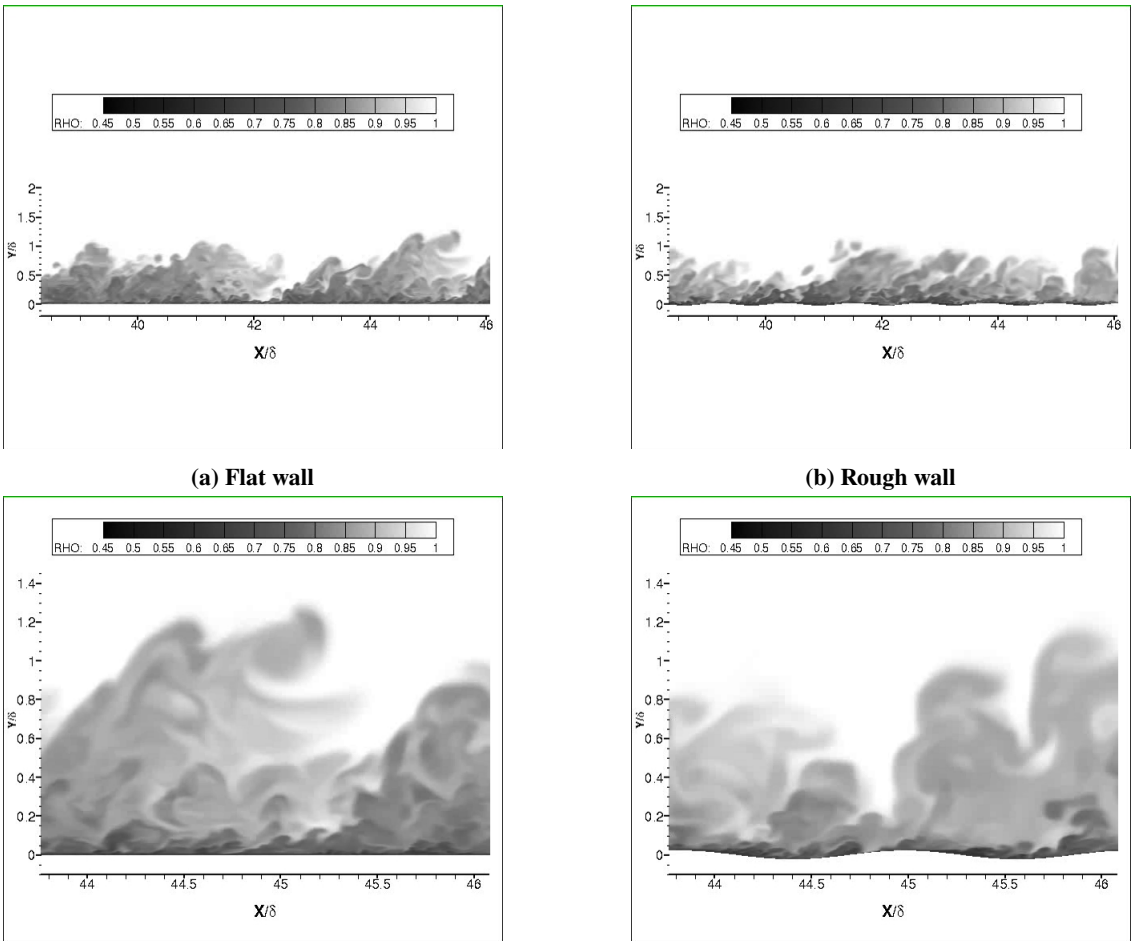

(a) Flat wall **(b) Rough wall**

(c) Flat wall close view **(d) Rough wall close view**

Fig. 2 Density contours of x-y plane in flowfield (ρ/ρ_∞).

Visualizing the flows into movie files shows active regions of turbulence in the valleys of the roughness elements. The windward region of the roughness elements appears to shelter the leeward region from turbulent generation, which is then taken downstream. Active regions of turbulence tend to be present in adverse pressure gradients. To investigate the described effect, the pressure coefficient on the surface of the wall is shown in Fig. 3.

In Fig. 3 the coefficient of pressure is greater than 1.0 in the valleys of the roughness elements. This is an indication of the compressibility of the flow. The adverse pressure gradients here tend to encourage the production of turbulence. The pressure coefficients in the valleys of the roughness elements are consistent with what is seen in the visualized flow. The adverse gradient of the pressure in the valleys of the roughness elements is consistent with the generation of turbulence.

An area of interest, regarding the concerns of Jiménez [2], is whether the roughness elements will affect the normal processes of turbulence. Taking planar views in the wall normal plane and plotting contours of velocity or density will show streaks of fluid consistent with the near-wall region. Streaks of dark fluid are normally associated with streamwise vortices which eventually grow to large-scale structures. Contours of streamwise velocity can be seen in Fig. 4. The y^+ locations chosen were those which showed peak streamwise Reynolds stress values. In the flat-wall case, Fig. 4a, typical streaks of high and low-speed fluid can be seen. These streaks were also seen by Pirozzoli and Bernardini [17]. In the rough-wall case 4b, the streaks are much less evident. A cross-section of the roughness elements can be seen disturbing this layer. The leeward portion of the roughness elements exhibits some of the streaks which are expected, prior to disruption of development of the streaks by the next roughness element. A sinusoidal plane was also plotted which maintains a constant wall-normal distance from the roughness elements. Some of the streaking pattern is recovered if the contours are plotted this way. For the rough-wall case, there is a secondary peak in streamwise Reynolds stress

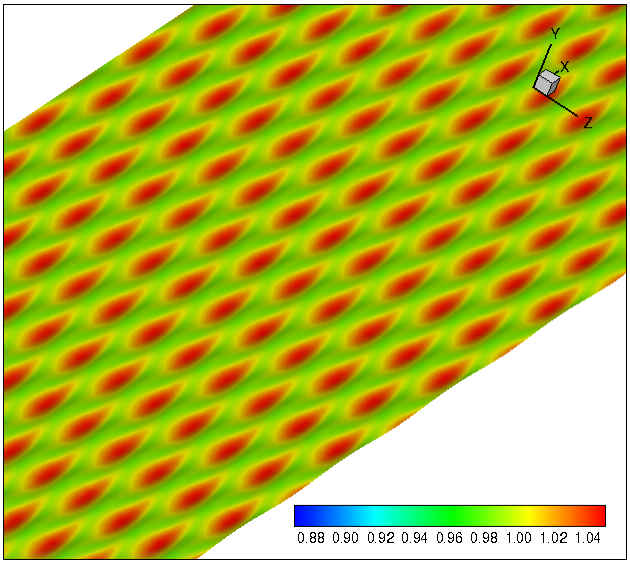

Fig. 3 Coefficent of pressure on the rough-wall surface. Valleys are red while the peaks are green.

at $y^+ = 88$. The location of the secondary peak of the Reynolds stress coincides with the tip of roughness elements. Contours of the streamwise velocity at the peak of the roughness elements can be seen in Fig. 4d. At the peaks, some of the streak behavior is recovered. The tip of the roughness elements act as sources of low-speed fluid which meet the inflow of freestream fluid.

An observation of the visualization of the flow of the fluid was a difference in the scales of the turbulent structures. To quantify this observation, two-point correlations of fluctuating velocities were calculated at several different wall-normal locations. The streamwise location selected coincided with the valley of a roughness element and was set as the x-origin. The contours of correlation values can be seen in Fig. 5. In this plot, δ represents the boundary layer thickness at $x/\delta_0 = 100$. In the region nearest to the wall ($\delta < 0.1$), there is a significant size difference between the flat and rough-wall turbulent structures. The rough-wall turbulent structures grow in size in the wall-normal direction until they are comparable in size to the flat-wall case. At $\delta = 0.55$, the scale for the rough case appears to be slightly larger than that of the flat-wall case. In the contours shown, the angle of the turbulent structures remains relatively shallow (approximately 15 degrees). This is different than what is seen in the instantaneous density contours (Fig. 2 where the turbulent structures seem to have an approximately 45 degrees inclination from the wall.

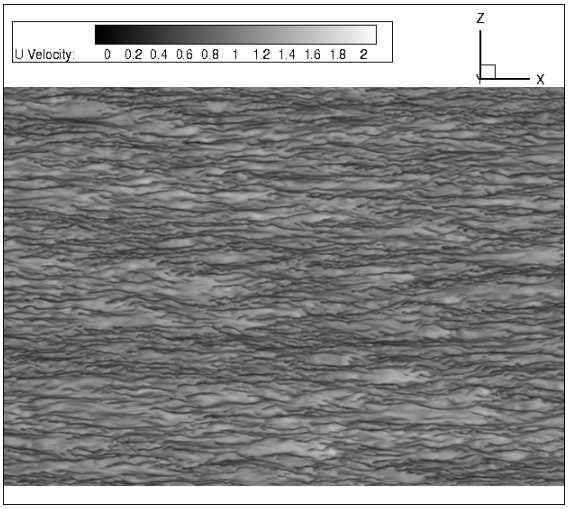

(a) Flat wall at $y^+ = 18$

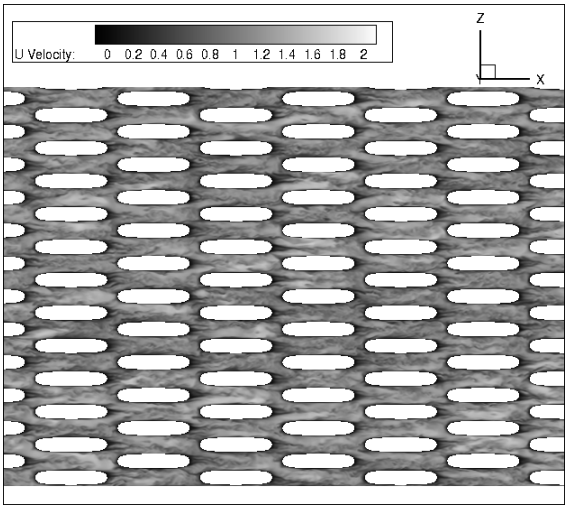

(b) Rough wall at $y^+ = 18$

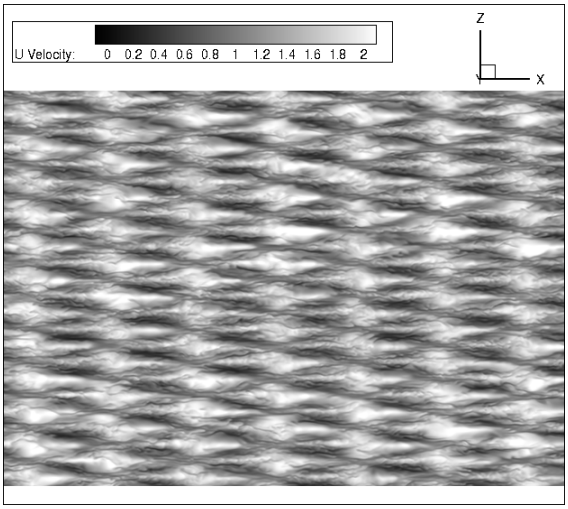

(c) Rough wall at $y^+ = 18$ following the curvature of the roughness elements

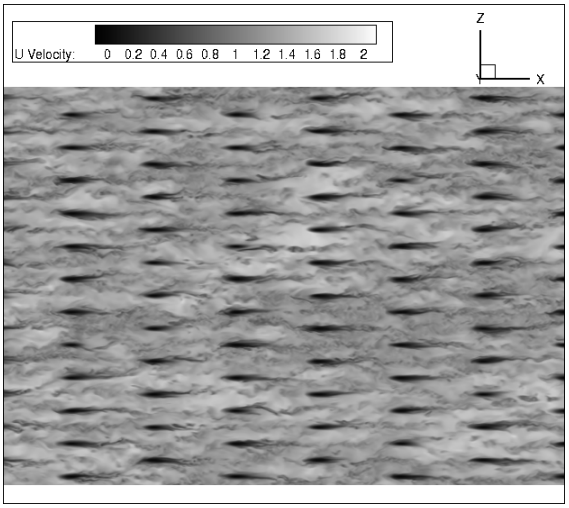

(d) Rough wall at $y^+ = 88$

Fig. 4 Streamwise (u) velocity contours in an x-z plane. Streaks typically seen in flat-wall boundary layers seem to be less evident in the rough-wall case.

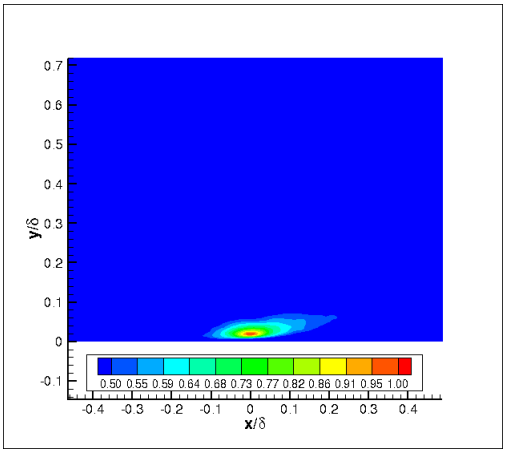

(a) Flat contour at $\delta = 0.02$

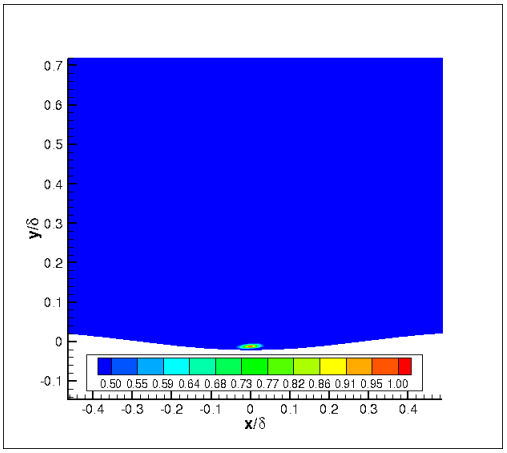

(b) Rough contour at $\delta = 0.02$

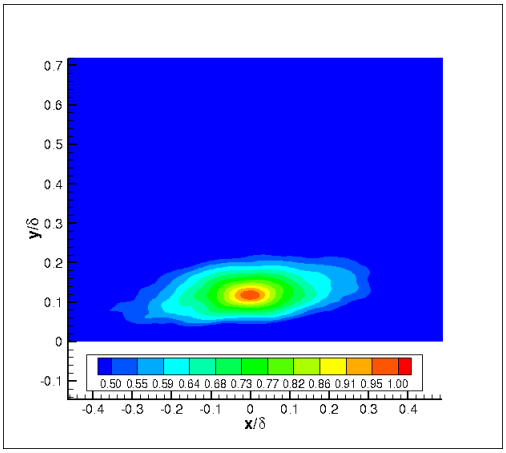

(c) Flat contour at $\delta = 0.12$

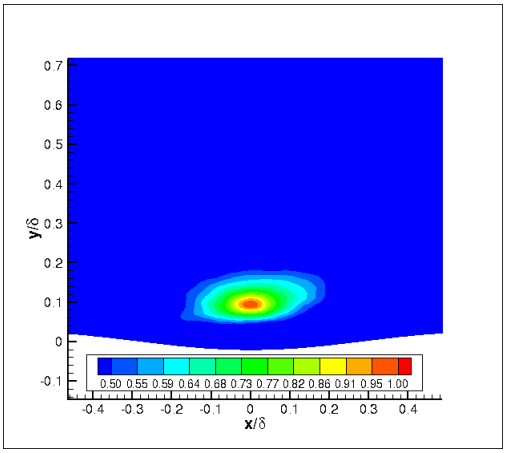

(d) Rough contour at $\delta = 0.12$

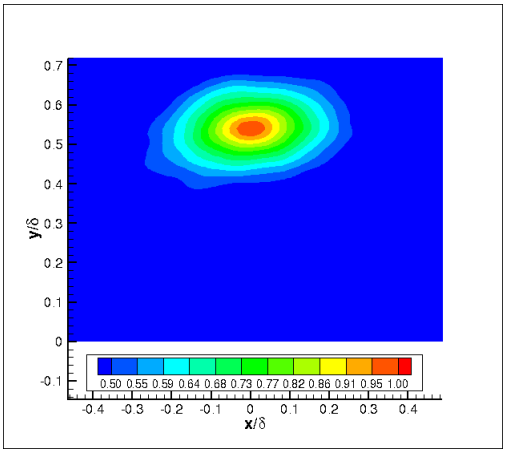

(e) Flat contour at $\delta = 0.55$

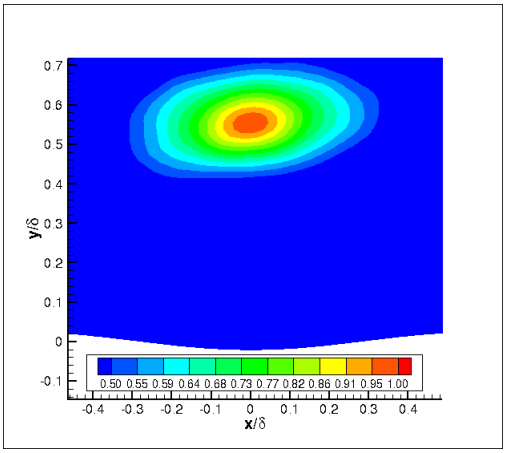

(f) Rough contour at $\delta = 0.55$

Fig. 5 Two-point correlations of streamwise velocity fluctuations ($\overline{u'u'}$). The rough-wall case shows smaller structures near the wall in the valley region and gradually increases when moving away from the wall to a comparable size of the structures in the flat-wall case.

The coefficient of friction for the rough-wall case is represented in a contour plot in Fig. 6. The windward side of the roughness elements shows higher values of skin friction than the valleys. This is expected as seen from Fig. 4. The front of the roughness elements shows higher speed fluid, increasing skin friction.

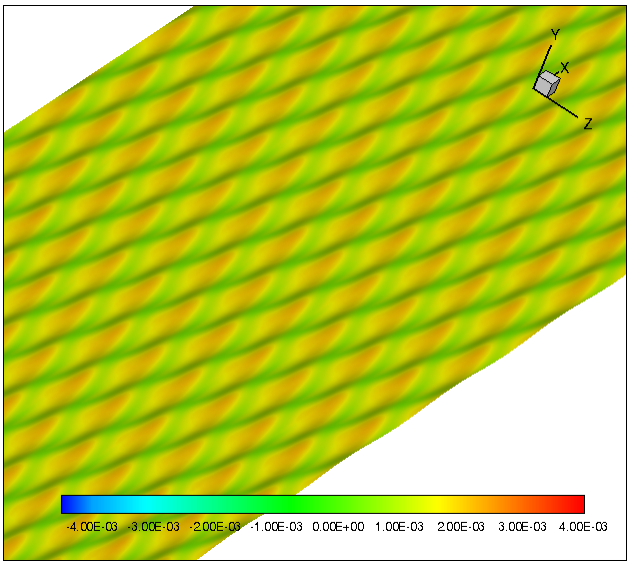

Fig. 6 Coefficient of friction on the rough-wall surface. The windward sides of the peaks are red which is indication of higher skin friction.

B. Mean Profiles

After first investigating the results visually, the results are investigated here for standard turbulence statistics. Figure 7 shows the spanwise averaged coefficient of friction for the length of the computational domain. The rough value of the coefficient of friction oscillates about the flat-wall value. At the end of the domain where $x/\delta = 100$, the mean rough value seems to dip lower than the mean flat value. The reference values of coefficient of friction used in calculating statistics were pulled from these plots at $x/\delta = 99$. Further investigation into the friction values is needed to determine why the mean value of the rough-wall case seems to dip below the flat-wall case at the end of the domain.

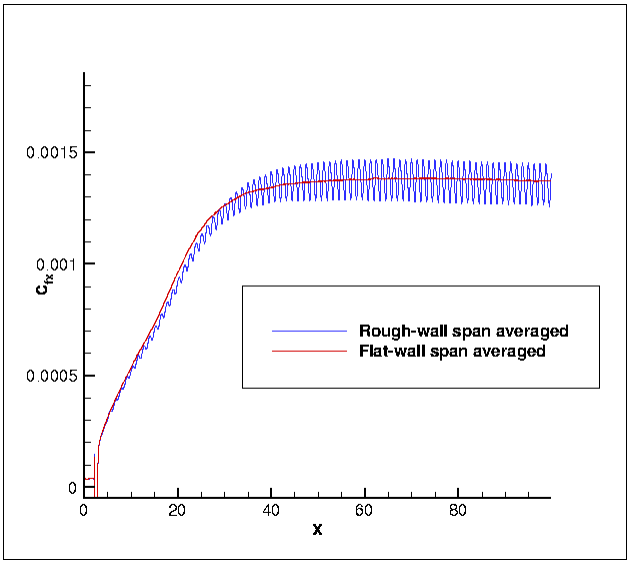

Fig. 7 Spanwise-averaged coefficient of friction. The rough-wall case oscillates about the flat-wall case

The mean velocity profile for the flow can be seen in Fig. 8. The velocity is scaled by the van Driest transformation to scale out density variation effects in compressible flow. Here the behavior of the downward shifted inner coordinates mean velocity profile is not seen as described by Peltier and Bowersox [13]. This could be due to the selected reference coefficient of friction. To evaluate whether the logarithmic behavior is retained by the flows, the diagnostic function ($\Xi = y^+(du^+_{vd}/dy^+)$), as referred to by Pirozzoli and Bernardini [17] was plotted and can be seen in Fig. 8b. There are some apparent logarithmic behaviors. The rough-wall case sees a large perturbation around $y^+ = 100$. This is consistent with the area directly above the peak of the roughness elements. The log law requires that the logarithmic region can be fit to the following equation:

$$u^+_{vd} = \frac{1}{\kappa} \ln y^+ + C \tag{6}$$

Here the value of κ for the rough-wall case is ≈ 0.34 and the value of C is ≈ 5.68 . For the flat-wall case the value of κ is ≈ 0.39 and the value of C is ≈ 8.45. Issues with these values could be due to the determination of reference coefficient of friction used to scale the values. The flat-wall values are similar to those seen by Pirozzoli and Bernardini [17]. The rough-wall case has a shifted value for κ, which could be an indication of the roughness elements disturbing the logarithmic layer. This could point towards the value of k/δ not being small enough in the current case study.

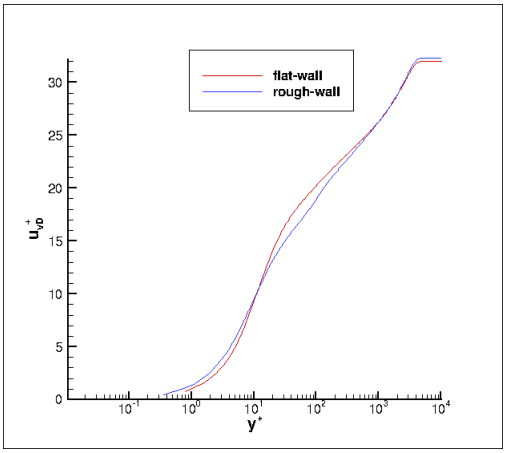

(a) Mean velocity profiles scaled with the van Driest transformation.

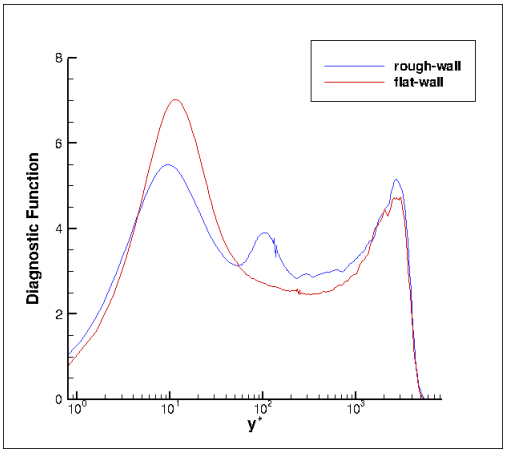

(b) Diagnostic function of mean velocity profiles.

Fig. 8 Mean velocity profile scaled by the van Driest transformation and the diagnostic function which is used to evaluate the logarithmic behavior. The rough-wall sees a deviation from the logarithmic behavior near the tip of the roughness elements.

Peltier and Bowersox [13] found the friction velocity using the Clauser chart method with van Driest compressibility scaling. This method uses the friction velocity as a course adjustment to match the mean velocity profiles with the universal log law. The effective origin is then used to fit the data with finer precision. This method is based on the assumption that the universal log law constant is $\kappa = 0.41$. Peltier and Bowersox [13] found that the Reynolds stresses were lower in magnitude when scaled by the friction velocity for the rough-wall case compared to the baseline smooth case. This contradicts the incompressible findings of Wu and Christensen [7][8][9] who found that Reynolds stresses collapsed to the same profiles when scaled by the friction velocity. The Reynolds stresses for both cases can be seen in Fig. 9. The streamwise Reynolds stress, Fig. 9a, partially exhibits the expected behavior of the rough case showing a Reynolds stress lower in magnitude. The remaining stresses, however, do not exhibit the same behavior. The rough-wall Reynolds stresses are often higher than the flat-wall case. The rough-wall stresses also exhibit secondary peaks, not characteristic of the smooth curves seen from the flat-wall case. These peaks coincide with the areas directly above the peak of the roughness elements. This could be a factor affecting the Reynolds stress values. Another possible issue is the choice of the reference coefficient of friction used to calculate the stresses. Further investigation is needed at this point.

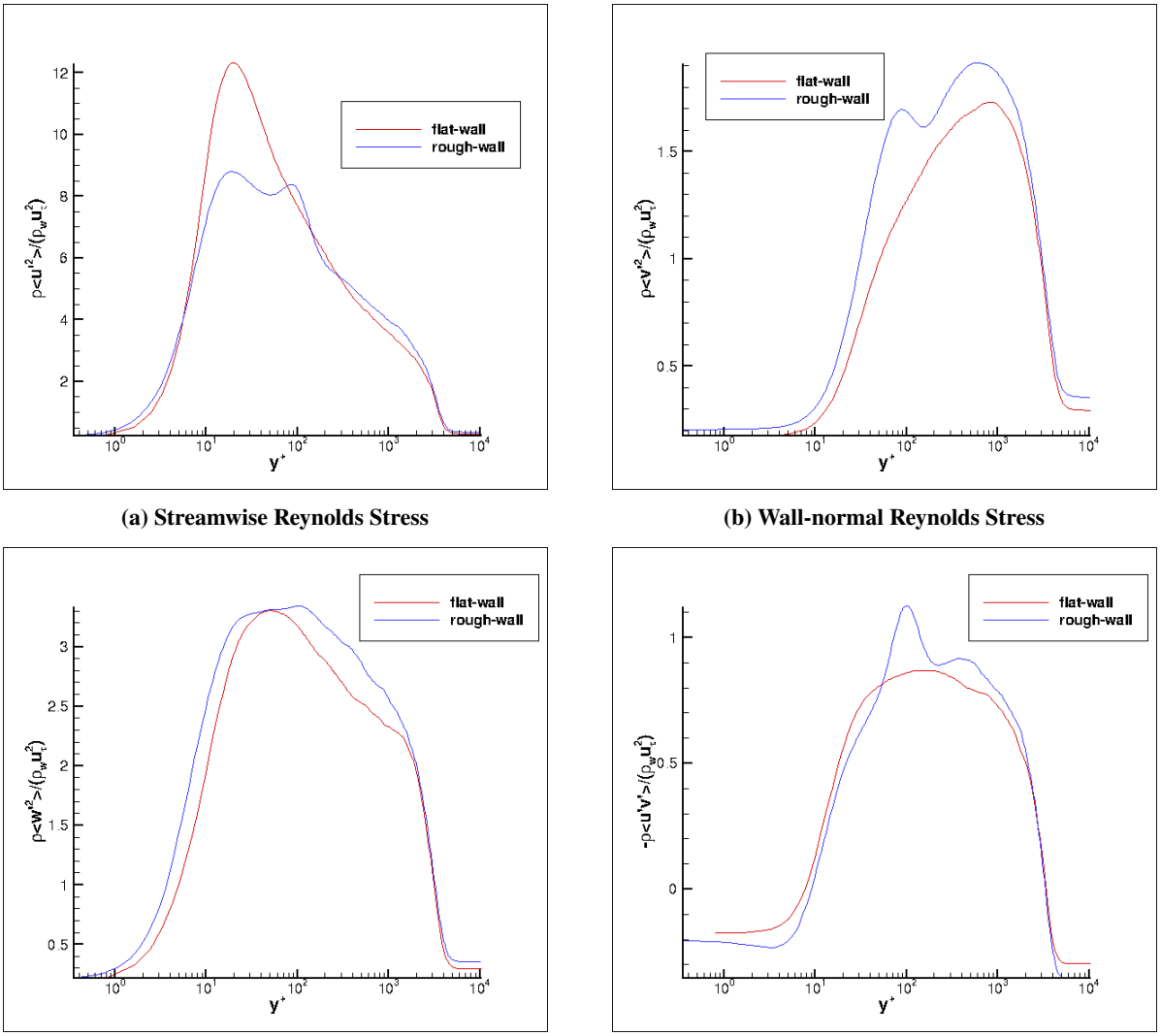

(a) Streamwise Reynolds Stress

(b) Wall-normal Reynolds Stress

(c) Spanwise Reynolds Stress

(d) Streamwise/Wall-normal Reynolds Stress

Fig. 9 Reynolds stresses for flat-wall and rough-wall case. The streamwise Reynolds stress exhibits the lower in magnitude expected, but the remaining stresses do not.

V. Conclusion

A computational study was conducted concerning the differences in flow physics between smooth and rough surfaces in compressible flow. Visual inspection of the flow reveals that the roughness elements tend to shelter generation of turbulence on the leeward side of peaks which is then expelled into the freestream. The rough surface also exhibits smaller turbulent length scales near the wall than the flat-wall case, but larger structures than the flat case near the boundary layer edge. Contour plots of streamwise velocity in horizontal planes reveal the streaks of high and low-speed fluid at the peak of the streamwise Reynolds stress in the flat-wall case. In the rough-wall case, the roughness elements directly interfere with this layer, and much of the streaking pattern is lost. In the aft portion of the roughness elements, the streaks seem to appear before they are interrupted by the next roughness element. A plot of a constant distance from the rough-wall shows that some of the streaking pattern is preserved when observing the flow with a constant wall-normal distance from the roughness. The peak of the roughness elements causes a secondary peak in the streamwise Reynolds stress. The peaks become sources of low-speed fluid, which mixes with the inflow of high-speed fluid.

The rough-wall streamwise Reynolds stress partially exhibits the expected behavior of lower magnitude values compared to the flat-wall case. The other rough-wall Reynolds stresses, however, do not exhibit the expected behavior of having lower magnitude than the flat case. The rough-wall stresses also show a secondary peak of which the roughness

elements are direct cause.

Further investigation is needed into proper selection of a reference coefficient of friction value for the scaling of the stresses. The secondary peak in the Reynolds stresses could also be an indication that the recommended value of k/δ by Jiménez [2] was not met. Future work will have to be conducted to increase the Reynolds number enough so that k^+ remains large enough while k/δ remains small enough. Investigation into other numerical options to reduce computational needs is ongoing.

Acknowledgments

This work was funded by the Air Force Research Laboratory, under the Multidisciplinary Hypersonics Program. Computer hours were provided by the DoD HPCMP. Approved for public release: distribution unlimited. Case Number: AFRL-2020-0416

References

[1] Bowersox, R., "Survey of High-Speed Rough Wall Boundary Layer:Invited Presentation," *37th AIAA Fluid Dynamics Conference and Exhibit*, 25 June 2007. https://doi.org/10.2514/6.2007-3998.

[2] Jiménez, J., "Turbulent Flows over Rough Walls," *Annual Review of Fluid Mechanics*, Vol. 36, No. 1, 2004, pp. 173–196. https://doi.org/10.1146/annurev.fluid.36.050802.122103, URL https://doi.org/10.1146/annurev.fluid.36.050802.122103.

[3] Jiménez, J., and Moin, P., "The minimal flow unit in near-wall turbulence," *Journal of Fluid Mechanics*, Vol. 225, 1991, p. 213–240. https://doi.org/10.1017/S0022112091002033.

[4] George, W. K., *Lectures in Turbulence for the 21st Century*, online resource, London, UK, 16 January 2013. URL http://www.turbulence-online.com/Publications/Lecture_Notes/Turbulence_Lille/TB_16January2013.pdf.

[5] Townsend, A., *The Structure of Turbulent Shear Flows*, 2nd ed., Cambridge Univ. Press, Cambridge, UK, 1976.

[6] Kocher, B. D., Combs, C. S., Kreth, P. A., and Schmisseur, J. D., "Characterizing the Streamwise Development of Surface Roughness Effects on a Supersonic Boundary Layer," *AIAA AVIATION Forum*, 25-29 June 2018. https://doi.org/10.2514/6.2018-4047, URL https://arc.aiaa.org/doi/abs/10.2514/6.2018-4047.

[7] WU, Y., and CHRISTENSEN, K. T., "Spatial structure of a turbulent boundary layer with irregular surface roughness," *Journal of Fluid Mechanics*, Vol. 655, 2010, p. 380–418. https://doi.org/10.1017/S0022112010000960.

[8] Wu, Y., and Christensen, K. T., "Reynolds-Stress Enhancement Associated with a Short Fetch of Roughness in Wall Turbulence," *AIAA Journal*, Vol. 44, No. 12, 2006, pp. 3098–3106. https://doi.org/10.2514/1.22357, URL https://doi.org/10.2514/1.22357.

[9] Wu, Y., and Christensen, K. T., "Outer-layer similarity in the presence of a practical rough-wall topography," *Physics of Fluids*, Vol. 19, No. 8, 2007, 085108. https://doi.org/10.1063/1.2741256, URL https://doi.org/10.1063/1.2741256.

[10] Latin, R. M., and Bowersox, R. D. W., "Flow Properties of a Supersonic Turbulent Boundary Layer with Wall Roughness," *AIAA Journal*, Vol. 38, No. 10, 2000, pp. 1804–1821. https://doi.org/10.2514/2.862, URL https://doi.org/10.2514/2.862.

[11] Latin, R. M., and Bowersox, R. D. W., "Temporal Turbulent Flow Structure for Supersonic Rough-Wall Boundary Layers," *AIAA Journal*, Vol. 40, No. 5, 2002, pp. 832–841. https://doi.org/10.2514/2.1749, URL https://doi.org/10.2514/2.1749.

[12] Ekoto, I. W., Bowersox, R. D. W., Beutner, T., and Goss, L., "Supersonic Boundary Layers with Periodic Surface Roughness," *AIAA Journal*, Vol. 46, No. 2, 2008, pp. 486–497. https://doi.org/10.2514/1.31729, URL https://doi.org/10.2514/1.31729.

[13] Peltier, S. J., Humble, R. A., and Bowersox, R. D. W., "Crosshatch roughness distortions on a hypersonic turbulent boundary layer," *Physics of Fluids*, Vol. 28, No. 4, 2016, 045105. https://doi.org/10.1063/1.4944657, URL https://doi.org/10.1063/1.4944657.

[14] Poggie, J., Bisek, N. J., and Gosse, R., "Resolution effects in compressible, turbulent boundary layer simulations," *Computers and Fluids*, Vol. 120, 2015, pp. 57 – 69. https://doi.org/https://doi.org/10.1016/j.compfluid.2015.07.015, URL http://www.sciencedirect.com/science/article/pii/S0045793015002492.

[15] Beam, R. M., and Warming, R. F., "An Implicit Factored Scheme for the Compressible Navier-Stokes Equations," *AIAA Journal*, Vol. 16, No. 4, 1978, pp. 393–402. https://doi.org/10.2514/3.60901, URL https://doi.org/10.2514/3.60901.

[16] Georgiadis, N. J., Rizzetta, D. P., and Fureby, C., "Large-Eddy Simulation: Current Capabilities, Recommended Practices, and Future Research," *AIAA Journal*, Vol. 48, No. 8, 2010, pp. 1772–1784. https://doi.org/10.2514/1.J050232, URL https://doi.org/10.2514/1.J050232.

[17] "Probing high-Reynolds-number effects in numerical boundary layers," *Physics of Fluids*, Vol. 25, No. 2, 2013, 021704. https://doi.org/10.1063/1.4792164, URL https://doi.org/10.1063/1.4792164.